

Symmetry-preserving calculation of pion light-front wave functions

Z.-Q. Yao (姚照千)^{ID,1,*} Z.-N. Xu (徐珍妮)^{ID,2,†}
 Y.-Y. Xiao (肖宇洋)^{ID,3,4} C. D. Roberts^{ID,3,4,‡} and J. Rodríguez-Quintero^{ID2}

¹*Helmholtz-Zentrum Dresden-Rossendorf, Bautzner Landstraße 400, D-01328 Dresden, Germany*

²*Dpto. Ciencias Integradas, Centro de Estudios Avanzados en Fis., Mat. y Comp.,*

Fac. Ciencias Experimentales, Universidad de Huelva, E-21071 Huelva, Spain

³*School of Physics, Nanjing University, Nanjing, Jiangsu 210093, China*

⁴*Institute for Nonperturbative Physics, Nanjing University, Nanjing, Jiangsu 210093, China*

(Dated: 2025 December 15)

Poincaré-covariant Bethe-Salpeter wave functions are used to calculate light-front wave functions (LFWFs) of the pion, π , and an analogue state, $\pi_{s\bar{s}}$. The current masses of the degenerate valence constituents in the $\pi_{s\bar{s}}$ are around 25-times larger than those of the pion's valence constituents. Both valence spin-antialigned ($\mathcal{L} = 0$) and valence spin-aligned ($\mathcal{L} = 1$) components are obtained and combined to produce the complete LFWF for each system. Comparing predictions delivered by two distinct Bethe-Salpeter kernels, the impact of nonperturbative dynamical effects contained in the more sophisticated (bRL) kernel are seen to be significant; and contrasts between π , $\pi_{s\bar{s}}$ results reveal the interplay between emergent hadron mass and mass effects owing to Higgs-boson couplings. Amongst the results, one finds that for π , $\pi_{s\bar{s}}$, the LFWFs can be approximated by a separable form, with that representation being pointwise reliable in the bRL cases. Moreover, the $\mathcal{L} = 1$ component is important; so a LFWF obtained after omission of this piece is typically a poor representation of the system. These features are naturally expressed in π , $\pi_{s\bar{s}}$ transverse momentum dependent parton distribution functions (TMDs). In this connection, it is found that a Gaussian *Ansatz* can only provide a rough guide to TMD pointwise behaviour: magnitude deviations between *Ansatz* and prediction exceed a factor of two on $k_1^2 \gtrsim 0.55 \text{ GeV}^2$. One should therefore be cautious in interpreting conclusions drawn from phenomenological analyses based upon Gaussian *Ansätze*.

I. INTRODUCTION

The pion is Nature's most fundamental Nambu-Goldstone boson. It is also the lightest strongly interacting particle, *viz.* a meson built from light valence quark + antiquark degrees of freedom. Resolving this dichotomy has long been a goal of high-energy nuclear and particle physics. Now, with the dawning of an era of high-energy, high-luminosity facilities [1–8], it becomes realistic to think of producing detailed maps of pion structure and therewith validating modern theoretical pictures of the pion [9, 10]; so, an explanation of a basic feature of Nature may finally be within reach.

A path to an understanding of the structure of a quantum system is provided by the object's wave function. The Schrödinger wave function associated with a non-relativistic system is a probability amplitude. It can be computed using a Lippmann-Schwinger equation. In Poincaré-invariant quantum field theory (PIQFT), the equivalent of the latter is the Bethe-Salpeter equation [11]. However, owing to the special features of PIQFT – in particular, the loss of particle number conservation – the Poincaré-covariant Bethe-Salpeter wave function does not admit interpretation as a probability amplitude.

In quantum field theory, a clean analogue of the Schrödinger wave function is provided by the light-front

wave function (LFWF) [10, Sec. 3A], [12]. Notably, for any system described by a Poincaré-covariant wave function, χ , the associated LFWF can be obtained via projection of χ onto the light front [13]. In hadron physics applications, this approach was shown to be practicable in Ref. [14] and it has since been widely used. Herein, we adapt the scheme to the calculation of the LFWF of the pion, π , and a (fictitious) analogue state, $\pi_{s\bar{s}}$, built from valence degrees of freedom with degenerate current-masses that are inflated to match that of the strange, s , quark. Using these LFWFs, we then proceed to deliver results for the helicity-independent transverse momentum dependent parton distribution function (TMD) of each system. Whilst a system's LFWF is not directly accessible, it is anticipated that existing and future accelerators will deliver precise data that enable empirical inference of the pion TMD [6, 7].

Over the past forty-five years, many phenomenological models of pion LFWFs have been developed and employed; recent examples are discussed, *e.g.*, in Refs. [15–23]. In contrast, herein we employ continuum Schwinger function methods (CSMs) [24–26] to deliver parameter-free predictions for π , $\pi_{s\bar{s}}$ Poincaré-covariant wave functions, which we subsequently project onto the light front. A merit of this approach is the straightforward realisation of the pion as simultaneously both a Nambu-Goldstone mode and quark + antiquark bound state [27–31].

When employing CSMs, the wave function obtained depends on the kernel used to complete the Bethe-Salpeter equation. We therefore compare results calculated using two different symmetry-preserving,

* z.yao@hzdr.de

† zhenni.xu@dcu.uhu.es

‡ cdroberts@nju.edu.cn

systematically-improvable kernels. Namely, (I) the rainbow-ladder (RL) truncation, which is the leading-order approximation in the scheme introduced in Refs. [32, 33]; and (II) the nonperturbatively constructed extension (bRL) of that truncation elucidated and employed in Refs. [34–36]. These comparisons enable one to [10, 37–42]: highlight the expression of emergent hadron mass (EHM) in the pion LFWF and TMD; and consider aspects of the impact of constructive interference between EHM and Higgs-boson mass generating effects in the Standard Model.

We stress that the results discussed herein are to be interpreted as expressing meson structural properties at the hadron scale, $\zeta_{\mathcal{H}} < m_N$, m_N is the nucleon mass. At $\zeta_{\mathcal{H}}$, all properties of the hadron are carried by its quasiparticle valence degrees of freedom. Evolution to higher scales can be accomplished using the all-orders (AO) scheme, detailed in Ref. [43], which has proven efficacious in numerous applications.

Section II sketches the CSM calculation of meson Bethe-Salpeter amplitudes. Algebraic connections between these amplitudes and meson LFWFs are provided in Sec. III. A practical procedure for projecting the Bethe-Salpeter amplitudes onto the light-front is explained and employed in Sec. IV. Section V discusses the helicity-independent TMDs determined by the LFWFs thus obtained. Section VI provides a summary and perspective.

II. POINCARÉ-COVARIANT BETHE-SALPETER WAVE FUNCTIONS

Using CSMs, meson bound state problems are solved by considering a set of coupled gap and Bethe-Salpeter equations [24]. Practical implementations of the RL truncation can be traced from Ref. [28] and first steps beyond RL truncation are described in Refs. [29, 30]. In either case, two elements are key, *viz.* (a) the effective charge; and (b) the dressed gluon-quark vertex, $\Gamma_\nu(q, p)$.

As explained in Refs. [44–47], studies of the gauge sector in quantum chromodynamics (QCD) lead one to the following practicable form for the product of effective charge and gluon 2-point Schwinger function:

$$\tilde{G}(y) = \frac{8\pi^2}{\omega^4} D e^{-y/\omega^2} + \frac{8\pi^2 \gamma_m \mathcal{F}(y)}{\ln[\tau + (1 + y/\Lambda_{\text{QCD}}^2)^2]}, \quad (1)$$

where $\gamma_m = 12/25$, $\Lambda_{\text{QCD}} = 0.234 \text{ GeV}$, $\tau = e^2 - 1$, and $\mathcal{F}(y) = \{1 - \exp(-y/\Lambda_I^2)\}/y$, $\Lambda_I = 1 \text{ GeV}$.

Using Eq. (1), the kernel of the dressed-quark gap equation has the form ($l = (p - q)$, $y = l^2$) [28, 46]:

$$\tilde{G}(y) T_{\mu\nu}(l) [i\gamma_\mu \frac{\lambda^a}{2}]_{tr} [i\Gamma_\nu(q, p) \frac{\lambda^a}{2}]_{su}, \quad (2)$$

$l^2 T_{\mu\nu}(l) = l^2 \delta_{\mu\nu} - l_\mu l_\nu$. This tensor structure specifies Landau gauge, employed because, *inter alia*, it is a

TABLE I. Panel A. Quark current masses and interaction parameters, Eq. (1), used to calculate meson wave functions: rainbow ladder (RL); and beyond rainbow-ladder (bRL), Eq. (3). The strength of the bRL anomalous chromomagnetic moment is fixed by $a = 1.1$. Panel B. Meson masses and leptonic decay constants obtained using the values in Panel A. Evolved at leading order to $\zeta = 2 \text{ GeV}$, the listed renormalisation group invariant current masses correspond to the following values (in GeV): RL – 0.0054, 0.121; bRL – 0.0031, 0.083. For context, Ref. [49, PDG] lists the following results: 0.0035, 0.094, values which align well with the bRL masses. (All tabulated quantities listed in GeV.)

| A | \hat{m} | \hat{m}_s | ω | $(\omega D)^{1/3}$ |
|-----|-----------|----------------------|----------|----------------------|
| RL | 0.0072 | 0.161 | 0.5 | 0.80 |
| bRL | 0.0041 | 0.110 | 0.8 | 0.72 |
| B | m_π | $m_{\pi_{s\bar{s}}}$ | f_π | $f_{\pi_{s\bar{s}}}$ |
| RL | 0.14 | 0.69 | 0.093 | 0.134 |
| bRL | 0.14 | 0.67 | 0.098 | 0.117 |

fixed point of the QCD renormalisation group. In solving all relevant Schwinger function equations, we use a mass-independent (chiral-limit) momentum-subtraction renormalisation scheme [48], with renormalisation scale $\zeta = 19 \text{ GeV}$. At this scale, the quark wave function renormalisation constants are practically unity, which is a practical merit. Evolution to different scales is straightforward.

In the context of Eq. (2), one may introduce RL truncation as [28, Sec. II] $\Gamma_\nu^{\text{RL}}(q, p) = \gamma_\nu$; then the EHM-improved bRL vertex employed in Refs. [35, 36] takes the following form:

$$\Gamma_\nu(q, p) = \Gamma_\nu^{\text{RL}}(q, p) - a \kappa(y) \sigma_{\alpha\nu} l_\alpha, \quad (3)$$

where $a = 1.1$ measures the strength of the associated EHM-induced dressed-quark anomalous chromomagnetic moment (ACM) term [50–53]. Since the ACM is nonperturbative, an IR-focused profile function is appropriate, *viz.* $\kappa(y) = (1/\omega) \exp(-y/\omega^2)$. Notably, in the hadron spectrum, the ACM improvement eliminates most defects of RL truncation results [35] and it is also known to have a discernible impact on hadron structure [36].

Using the quark current masses and parameter values in Table I A, one can solve the necessary gap and Bethe-Salpeter equations using what are now standard algorithms [28, 54, 55]. This yields the Bethe-Salpeter wave functions along with the meson masses and leptonic decay constants listed in Table I B. For the ground state pion, both RL and bRL predictions are a good match with empirical determinations [49]. This outcome is an implicit expression of the Nambu-Goldstone boson character of the pion [27–31]: all symmetry-preserving CSM truncations must deliver a good description. Regarding $\pi_{s\bar{s}}$, the meson masses are the same, but one sees a 15% difference between the decay constants. This is an indication of the observable impact of bRL corrections in the

neighbourhood of the s quark mass, *viz.* following this size of Higgs-boson induced shift away from the Nambu-Goldstone boson limit.

Widespread use has shown that when the product ωD is kept fixed, one typically finds that ground-state pseudoscalar meson observables remain practically unchanged under $\omega \rightarrow (1 \pm 0.1)\omega$ [26]. Thus, since the quark current-masses are fixed by the meson masses, then ω is the only real parameter in Table I A. It is fixed by requiring a realistic value of the π leptonic decay constant.

III. LFWF: FORMULAE

The Poincaré-covariant Bethe-Salpeter wave function for a pseudoscalar meson can be written in the form

$$\begin{aligned} \chi_5(k; P) = S(k_\eta) \{ & \gamma_5 [iE_5(k; p) + k \cdot P F_5(k; P) \\ & + k \cdot P \gamma \cdot k G_5(k; p) + \sigma_{\mu\nu} k_\mu P_\nu H_5(k; P)] \} S(k_{\bar{\eta}}), \end{aligned} \quad (4)$$

where S is the 2-point Schwinger function (propagator) associated with the valence degrees of freedom in the bound-state; P is the meson total momentum, $P^2 = -m_5^2$, with m_5 the meson mass; k is the relative momentum between the valence quark and antiquark whose properties specify the character of the system, and $k_\eta = k + \eta P$, $k_{\bar{\eta}} = k - (1 - \eta)P$, $0 \leq \eta \leq 1$. For mesons built from mass-degenerate valence degrees of freedom, it is useful to choose $\eta = 1/2$; then, E, F, G, H in Eq. (4) are even functions of $k \cdot P$. Projected into the rest-frame, the wave function in Eq. (4) describes a meson with both S- and P-wave orbital angular momentum components [56, 57]. In all subsequent calculations, the canonically normalised Bethe-Salpeter wave function is used; see, *e.g.*, Ref. [58, Sec. 3] for discussion of this normalisation definition.

A pseudoscalar meson LFWF has two components:

$$\begin{aligned} \psi_5^\mathcal{L}(x, k_\perp^2) \propto & \gamma_5 [\gamma \cdot n \psi_5^0(x, k_\perp^2) \\ & + i\sigma_{\mu\nu} n_\mu k_{\perp\nu} \psi_5^1(x, k_\perp^2)], \end{aligned} \quad (5)$$

where n is a lightlike 4-vector, $n^2 = 0$, $n \cdot k_\perp = 0$, and $n \cdot P = -m_5$ in the meson rest frame. The superscript on ψ indicates the light-front orbital angular momentum projection: the $\mathcal{L} = 0 = \uparrow\downarrow = \downarrow\uparrow$ wave function has the light-front spins of the valence constituents antialigned; and $\mathcal{L} = 1 = \uparrow\uparrow = \downarrow\downarrow$ has them aligned. In our conventions, the $\mathcal{L} = 0$ component has mass dimension $1/\text{GeV}$ and that of $\mathcal{L} = 1$ is $1/\text{GeV}^2$.

Working with Eq. (4), the independent components in Eq. (5) may be obtained via light-front projections:

$$\psi_5^\mathcal{L}(x, k_\perp^2) = \text{tr}_{\text{CD}} \int \frac{dk_3 dk_4}{\pi} \delta(xn \cdot P - n \cdot k_\eta) \mathcal{P}^\mathcal{L} \chi_5(k; P), \quad (6)$$

where the trace is over colour and spinor indices and

$$\mathcal{P}^0 = \frac{1}{4} \gamma_5 \gamma \cdot n, \quad \mathcal{P}^1 = \frac{1}{4} \frac{i}{k_\perp^2} \gamma_5 \sigma_{\mu\nu} n_\mu k_{\perp\nu}. \quad (7)$$

The leading-twist two quasiparticle distribution amplitude (DA), calculated in Ref. [14], is straightforwardly obtained from Eq. (6):

$$f_5 \varphi_5(x) = \int^\Lambda \frac{d^2 k_\perp}{16\pi^3} \psi_5^0(x, k_\perp^2), \quad (8)$$

where f_5 is the meson's leptonic decay constant and \int^Λ indicates that a translationally invariant regularisation scheme must be used to calculate what is now effectively a four-dimensional integral. The Mellin moments of this DA are plainly k_\perp^2 -independent.

The associated pseudoscalar meson helicity-independent TMD is even more straightforward:

$$f_1(x, k_\perp^2) = \frac{1}{(2\pi)^3} [|\psi_5^0(x, k_\perp^2)|^2 + k_\perp^2 |\psi_5^1(x, k_\perp^2)|^2], \quad (9)$$

from which follows the pseudoscalar meson valence quasiparticle distribution function:

$$q_5(x) = \int d^2 k f_1(x, k_\perp^2). \quad (10)$$

Since we are dealing with “isospin”-symmetric states, there is no need to distinguish between particle and antiparticle valence constituents. Normalisation of the LFWF is equivalent to baryon number conservation:

$$\int_0^1 dx q_5(x) = 1. \quad (11)$$

Here, it is worth reiterating that we deliver results at the hadron scale, $\zeta_{\mathcal{H}}$. This scale is defined in the context of QCD effective charges [59, 60], wherewith a QCD running coupling is defined using the expansion of a chosen observable restricted to first order in the perturbative coupling, α_s ; see the discussion in Ref. [61, Sec. 4.3]. It follows that effective charges are typically process dependent, *e.g.*, $\alpha_{g_1}(k^2)$, defined via the Bjorken sum rule [62]. Any such coupling is analogous to the Gell-Mann–Low coupling in quantum electrodynamics [63] and has the following properties: the coupling is consistent with the QCD renormalisation group; renormalisation scheme independent; everywhere analytic and finite; and provides an infrared completion of any perturbatively-defined (standard) running coupling.

We adopt the effective charge elucidated in Ref. [43], denoted $\alpha_{1\ell}(k^2)$. This is a function which, when used to integrate the leading-order perturbative DGLAP equations [64–67], defines an evolution scheme for all parton distribution functions (DFs) and for any hadron that is all-orders exact. This is the all-orders (AO) approach. Its definition is broader than usual because it refers to an entire class of observables, not just a single measurable quantity. We stress that the pointwise form $\alpha_{1\ell}(k^2)$ is largely irrelevant given that a large number of model-independent results can be proved without any reference to the k^2 -profile of $\alpha_{1\ell}(k^2)$; see, *e.g.*, Refs. [47, 68–71]

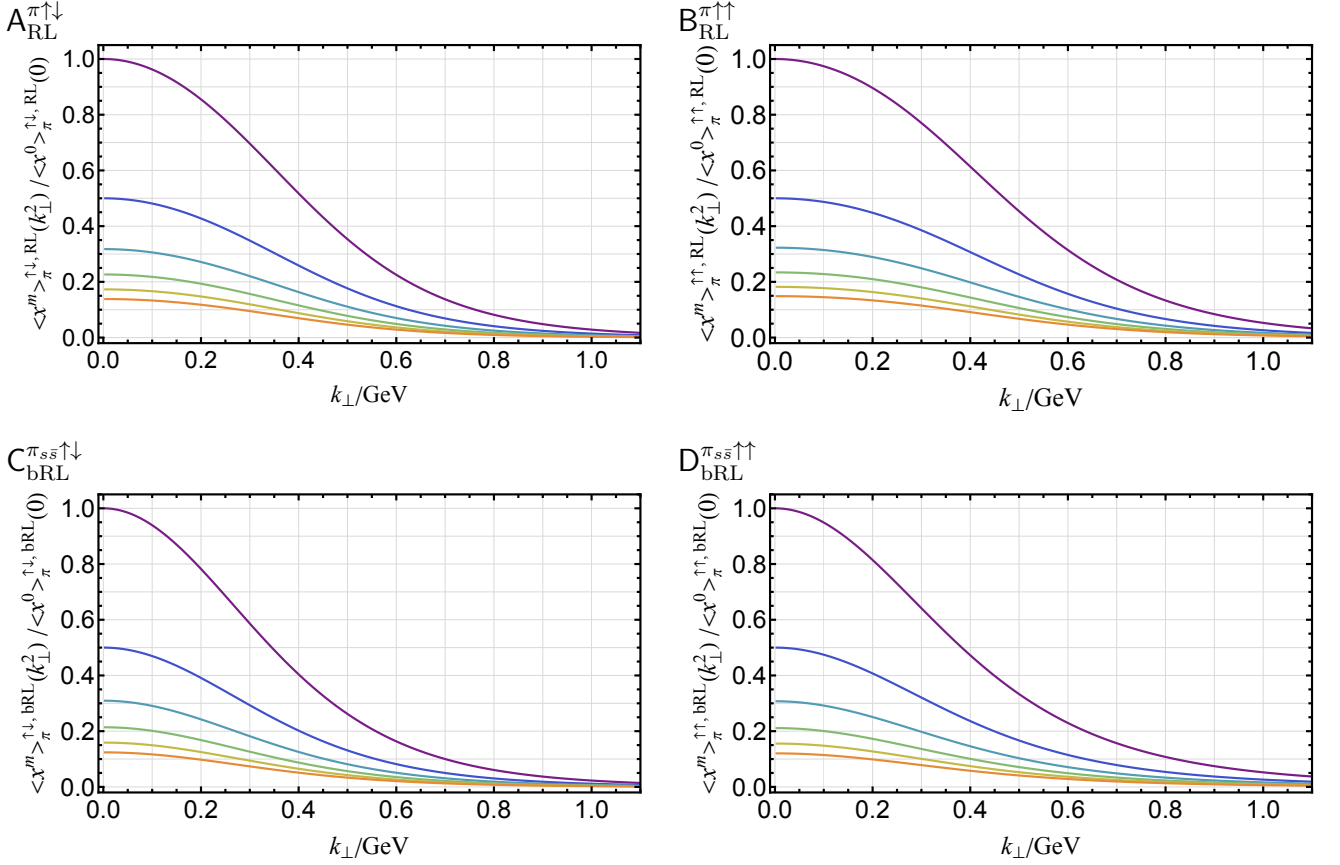


FIG. 1. Mellin moments, $m = 0, \dots, 5$, of π LFWF, defined by Eq. (12): the magnitudes decrease with increasing m . Panel A. RL, spins antialigned, $\langle x^0 \rangle_{\pi}^{\uparrow\downarrow}(0) = 55.9/\Lambda_I$. Panel B. RL, spins aligned, $\langle x^0 \rangle_{\pi}^{\uparrow\uparrow}(0) = (9.61/\Lambda_I)^2$. Panel C. bRL, spins antialigned, $\langle x^0 \rangle_{\pi}^{\uparrow\downarrow}(0) = 72.5/\Lambda_I$. Panel D. bRL, spins aligned. $\langle x^0 \rangle_{\pi}^{\uparrow\uparrow}(0) = (12.8/\Lambda_I)^2$. (Recall $\Lambda_I = 1 \text{ GeV}$, Eq. (1).)

Hereafter we exploit the fact that, with an effective charge defined in this way, there is a resolving scale, $\zeta = \zeta_{\mathcal{H}} < m_N$, at which all properties of a given hadron are carried by its dressed valence degrees of freedom. Consequently, the LFWFs and TMDs determined herein are expressed with reference to a quasiparticle Fock space defined by a light-front Hamiltonian that corresponds to the CSM truncations described above. Since the LFWFs are obtained by light-front projection of a given Poincaré-covariant Bethe-Salpeter wave function, then the Hamiltonian need not be specified. It is sufficient to record here that the leading component in the quasiparticle Fock space consists of an enumerable infinity of gluon, quark, and antiquark parton Fock space vectors.

IV. LFWF: RESULTS

Direct evaluation of the integrals specified by Eq (6) would require detailed knowledge of $\mathcal{X}_5(k; P)$ in the complex- k_{η}^2 plane. That need can be circumvented by working with the following k_{\perp}^2 -dependent Mellin mo-

ments:

$$\langle x^m \rangle^{\mathcal{L}}(k_{\perp}^2) = \int_0^1 dx x^m \psi_5^{\mathcal{L}}(x, k_{\perp}^2) \quad (12a)$$

$$= \frac{1}{n \cdot P} \text{tr}_{\text{CD}} \int \frac{dk_3 dk_4}{\pi} \left[\frac{n \cdot k_{\eta}}{n \cdot P} \right]^m \mathcal{P}^{\mathcal{L}} \mathcal{X}_5(k; P). \quad (12b)$$

We calculate these moments using the approach discussed in connection with Ref. [36, Eq. (15)]; and, furthermore, reexpress the measure and integrand in polar coordinates. The latter step works to improve the precision of interpolations used in the numerical integration. Following this prescription, stable results for the k_{\perp}^2 -dependence of moments $m = 0, 1, \dots, 5$ are readily obtained.

In reconstructing a LFWF from this set of moments, a systematic uncertainty is introduced by neglecting $m \geq 6$; but it is small so long as flexible, physically constrained reconstruction functions are chosen; see, *e.g.*, Refs. [14, 68, 71–73].

The calculated moments are drawn in Fig. 1. Comparing upper with lower panels, one sees that the RL LFWF moments exhibit a slower fall-off with k_{\perp}^2 than the bRL moments. Hence, the RL LFWF must be broader in k_{\perp} -

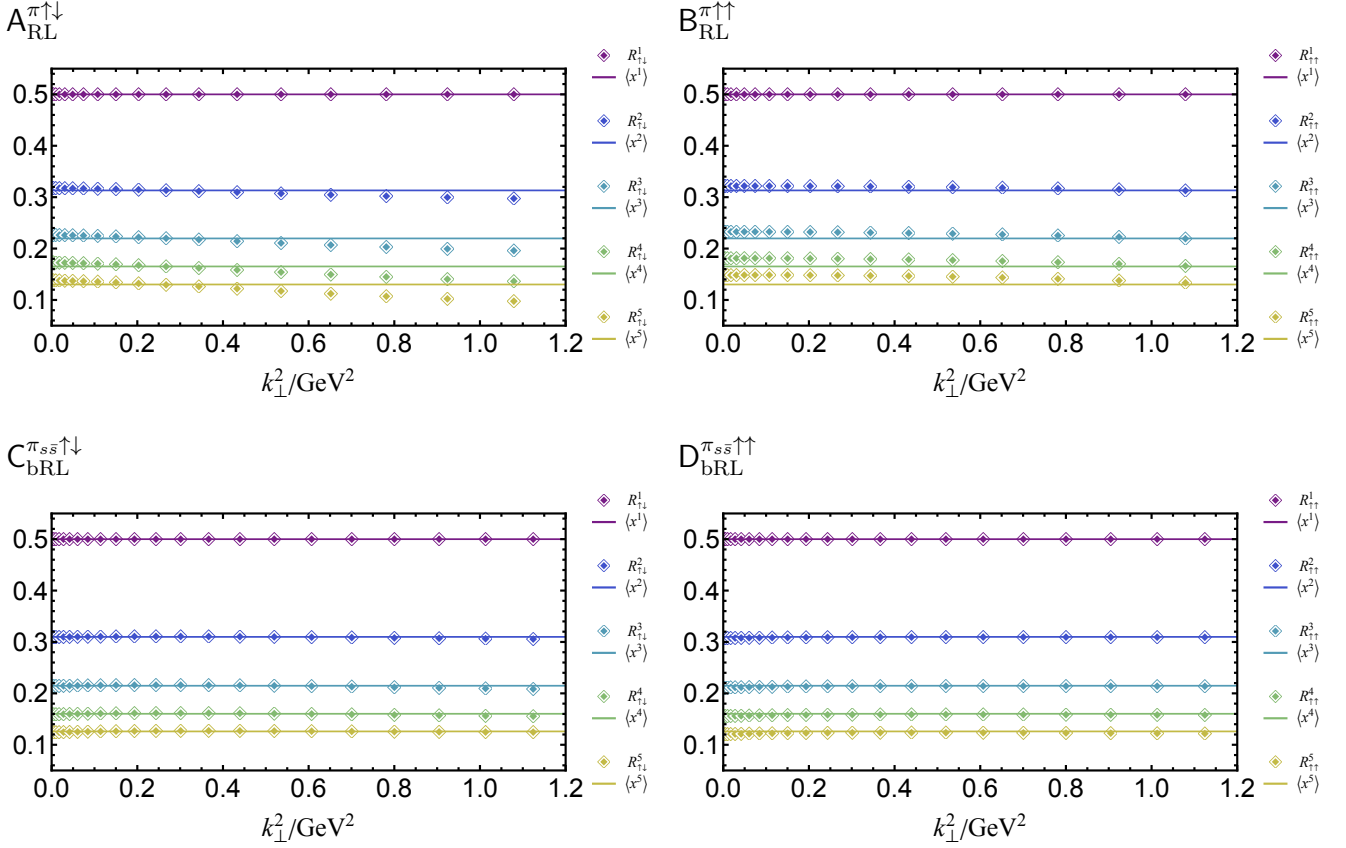


FIG. 2. Ratios of LFWF Mellin moments, Eq. (13). In each panel, the solid lines mark the k_\perp^2 -independent m moment of the DA in Eq. (8). Panel A. RL, spins antialigned. Panel B. RL, spins aligned. Panel C. bRL, spins antialigned. Panel D. bRL, spins aligned.

space or, equally, more pointlike in the conjugate configuration space. It follows, moreover, that the RL DA, Eq. (8), must also be broader than the bRL DA. This result was first reported in Ref. [14]. The conclusion is supported by numerical simulations of lattice-regularised QCD (IQCD) [74].

In Fig. 2, we plot the following dimensionless ratios:

$$R_\pi^{m, \mathcal{L}}(k_\perp^2) = \frac{\langle x^m \rangle_\pi^{\mathcal{L}}(k_\perp^2)}{\langle x^0 \rangle_\pi^{\mathcal{L}}(k_\perp^2)}. \quad (13)$$

Considering the RL results, Figs. 2 A, B, one sees that the ratio is k_\perp^2 -independent to a fair degree and the value for each moment is close to that of the analogous moment obtained from the DA in Eq. (8). Furthermore, the ratios for both spin projections are practically equivalent. One can therefore conclude that the RL pion LFWF – both spin components – can approximately be written in a factorised form:

$$\psi_5^{\mathcal{L}}(x, k_\perp^2) \approx \varphi_5(x) \times F^{\mathcal{L}}(k_\perp^2). \quad (14)$$

Importantly, the images indicate that both spin projections have the same x -dependence, *i.e.*, are characterised by the same DA; see, also, Appendix A – Table III. As

explained and exploited, *e.g.*, in Refs. [10, Sec. 3], [73], [75], it follows that Eq. (10) entails

$$q_5(x) \propto \varphi_5^2(x), \quad (15)$$

notwithstanding the presence of the LFWF $\mathcal{L} = 1$ component.

On the other hand, analyses in perturbative QCD predict [76]:

$$k^2 \gg m_N^2 \mid \psi_5^0(x, k_\perp^2) \propto \frac{1}{k_\perp^2} \propto k_\perp^2 \psi_5^1(x, k_\perp^2), \quad (16)$$

up to (damping) $\ln k_\perp^2$ corrections. CSM predictions are consistent with this behaviour. Consequently, realistic representations of LFWF k_\perp^2 dependence must express different ultraviolet behaviour for the independent spin projections.

Turning to ratio results obtained with the EHM-improved bRL kernel, Figs. 2 C, D, one sees that what were approximately k_\perp^2 -independent profiles in RL truncation, which were reasonably well matched with the associated DA moment, become constant profiles with k_\perp^2 -independent values that are practically indistinguishable

from the linked DA moment. Thus whilst Eq. (14) provides a fair approximation to the RL results, it delivers a reliable pointwise representation for the bRL pion LFWF. (See, also, Appendix A – Table III.)

Qualitatively equivalent statements can be made about the $\pi_{s\bar{s}}$ moments and LFWFs.

The results described above provide strong support for the approach to calculating pion and kaon DFs and generalised parton distributions in, *e.g.*, Refs. [73, 75].

Having established that separable *Ansätze* provide a sound representation of π , $\pi_{s\bar{s}}$ LFWFs, we introduce a particular form of Eq. (14), *viz.*

$$\psi_5^\mathcal{L}(x, k_\perp^2) = \varphi_5(x) \times p_5^\mathcal{L}(k_\perp^2), \quad (17)$$

with

$$\varphi_5(x) = \frac{1}{N} \ln[1 + x(1-x)/\rho_5^2], \quad (18)$$

where ρ_5 is a constant, N ensures $\int_0^1 dx \varphi_5(x) = 1$, consistent with Eq. (8), and

$$p_5^\mathcal{L}(k_\perp^2) = p_{5R}^\mathcal{L}(k_\perp^2) + p_{5V}^\mathcal{L}(k_\perp^2), \quad (19a)$$

$$p_{5R}^\mathcal{L}(k_\perp^2) = \frac{a_0^\mathcal{L}/\Lambda_I^{1+\mathcal{L}}}{1 + b_1^\mathcal{L}k_\perp^2/\Lambda_I^2 + b_2^\mathcal{L}k_\perp^4/\Lambda_I^4}, \quad (19b)$$

$$p_{5V}^\mathcal{L}(k_\perp^2) = \frac{c_0^\mathcal{L}/\Lambda_I^{1+\mathcal{L}}}{1 + d_1^\mathcal{L}k_\perp^2/\Lambda_I^2}. \quad (19c)$$

Notably, for any $\rho_5 \gtrsim 1$ in Eq. (18), the x -profile of $\psi_5^\mathcal{L}(x, k_\perp^2)$ is essentially equivalent to that of the QCD asymptotic DA [76–78]: $\varphi_{as}(x) = 6x(1-x)$. Indeed, using the L_1 measure, the curves obtained with $\rho_5 = 1, 2$ differ by just 1.4%, with $\rho_5 = 2$ differing from φ_{as} by just 0.52%. Moreover, in order to ensure reconstruction consistency with Eq. (16), two independent Padé approximants are used to express $p_5^\mathcal{L}(k_\perp^2)$. For $\mathcal{L} = 0$, all five reconstruction parameters are nonzero in the k_\perp^2 term; but for $\mathcal{L} = 1$, $c_0^\mathcal{L} = 1 \equiv 0 \Rightarrow p_{5V}^{\mathcal{L}=1} \equiv 0$, *viz.* there are only three parameters.

Using this product *Ansatz* and the least-squares fitting procedure described in Appendix A, one arrives at the dimensionless best-fit reconstruction parameters listed in Table II. The entry ρ_{as} means that, within any sensible understanding of the precision that may be achieved, the x -profile is indistinguishable from φ_{as} . As noted above, any value $\rho \gtrsim 1$ is practically equivalent in this case. The associated correlation matrices are listed in Appendix A.

Using the central values in Table II, one produces the LFWF images in Fig. 3. The following points are worth stressing.

- (i) In each case, comparing kindred RL and bRL results, a given RL LFWF damps less rapidly as the probe is moved in any direction away from its global maximum, *i.e.*, RL LFWFs are (far) more dilated than bRL LFWFs. (Reference [14] demonstrated this for DAs.) Consequently, RL truncation produces a bound-state that is more

TABLE II. Values of LFWF coefficients in Eq. (17) for the various truncations and systems considered herein. *N.B.* In all cases, within mutual uncertainties, $\rho^{(0=\uparrow\downarrow)} = \rho^{(1=\uparrow\uparrow)}$. Associated correlation matrices are collected in Appendix A.

| $p_{5R}^\mathcal{L}$ | $a_0^\mathcal{L}$ | $b_1^\mathcal{L}$ | $b_2^\mathcal{L}$ | $\rho^{(\mathcal{L})}$ |
|--|-------------------|-------------------|-------------------|------------------------|
| $\psi_{\pi, \text{RL}}^{\uparrow\downarrow}$ | 51.21(2.85) | 1.83(60) | 20.45(1.18) | 0.086(12) |
| $\psi_{\pi, \text{RL}}^{\uparrow\uparrow}$ | 91.98(0.24) | 1.99(09) | 12.21(0.34) | 0.031(04) |
| $\psi_{\pi, \text{bRL}}^{\uparrow\downarrow}$ | 67.76(3.13) | 4.41(63) | 26.14(1.35) | 0.224(19) |
| $\psi_{\pi, \text{bRL}}^{\uparrow\uparrow}$ | 164.30(0.24) | 5.04(07) | 12.20(0.26) | 0.285(11) |
| $\psi_{\pi_{s\bar{s}}, \text{RL}}^{\uparrow\downarrow}$ | 39.98(2.52) | 0.78(41) | 8.31(0.52) | ρ_{as} |
| $\psi_{\pi_{s\bar{s}}, \text{RL}}^{\uparrow\uparrow}$ | 49.39(0.23) | 1.11(10) | 5.46(0.25) | ρ_{as} |
| $\psi_{\pi_{s\bar{s}}, \text{bRL}}^{\uparrow\downarrow}$ | 70.47(3.36) | 3.56(57) | 20.70(1.10) | ρ_{as} |
| $\psi_{\pi_{s\bar{s}}, \text{bRL}}^{\uparrow\uparrow}$ | 136.29(0.25) | 4.12(08) | 11.72(0.31) | ρ_{as} |
| $p_{5V}^\mathcal{L}$ | $c_0^\mathcal{L}$ | $d_1^\mathcal{L}$ | | |
| $\psi_{\pi, \text{RL}}^{\uparrow\downarrow}$ | 4.87(2.91) | 48.24(29.98) | | |
| $\psi_{\pi, \text{bRL}}^{\uparrow\downarrow}$ | 4.89(3.18) | 60.80(37.30) | | |
| $\psi_{\pi_{s\bar{s}}, \text{RL}}^{\uparrow\downarrow}$ | 4.77(2.57) | 30.45(17.05) | | |
| $\psi_{\pi_{s\bar{s}}, \text{bRL}}^{\uparrow\downarrow}$ | 5.34(3.42) | 52.50(31.90) | | |

compact in the conjugate coordinate space than the bRL kernel. Available comparisons with inferences from data and other robust calculations indicate that bRL results are more realistic; see, *e.g.*, Refs. [35, 36, 68, 73, 79–81]. Thus the true extent of LFWFs is best measured by the bRL predictions.

- (ii) With increased quark current mass, the x dependence of each LFWF is less dilated. The reduced dilation, *i.e.*, contraction, is an expression in the DA of Higgs-boson modulation of EHM. In fact, as revealed in Refs. [37, 82–84], confirmed via lQCD [85], and reproduced by our analysis, the $\pi_{s\bar{s}}$ DA is practically indistinguishable from the QCD asymptotic DA [76–78]: $\varphi_{\pi_{s\bar{s}}} \approx \varphi_{as}$.
- (iii) Regarding the LFWF k_\perp^2 dependence, the images in Fig. 3 paint an ambiguous picture. On the domain depicted, with increased quark current-mass, RL truncation obviously delivers results with dilated k_\perp^2 profiles. In contrast, the k_\perp^2 profiles of the more realistic bRL LFWFs are fairly insensitive to the change in quark current mass.

To understand and resolve the ambiguity highlighted in (iii), it is necessary to consider the k_\perp^2 dependence on a larger domain; see Fig. 4. Considering these profiles, obtained after rescaling such that $\psi_n^0(1/2, 0)$ is unity for each quark current mass, then one then observes the following.

- (a) Compare the k_\perp^2 -profiles of $\psi_n^0(x, k_\perp^2)$. Plainly, RL truncation produces a more dilated function than bRL on the entire k_\perp^2 domain. Considering $|k_\perp| |\psi_n^1(x, k_\perp^2)|$, on the other hand, RL truncation yields narrower (contracted) k_\perp^2 profiles. Evidently,

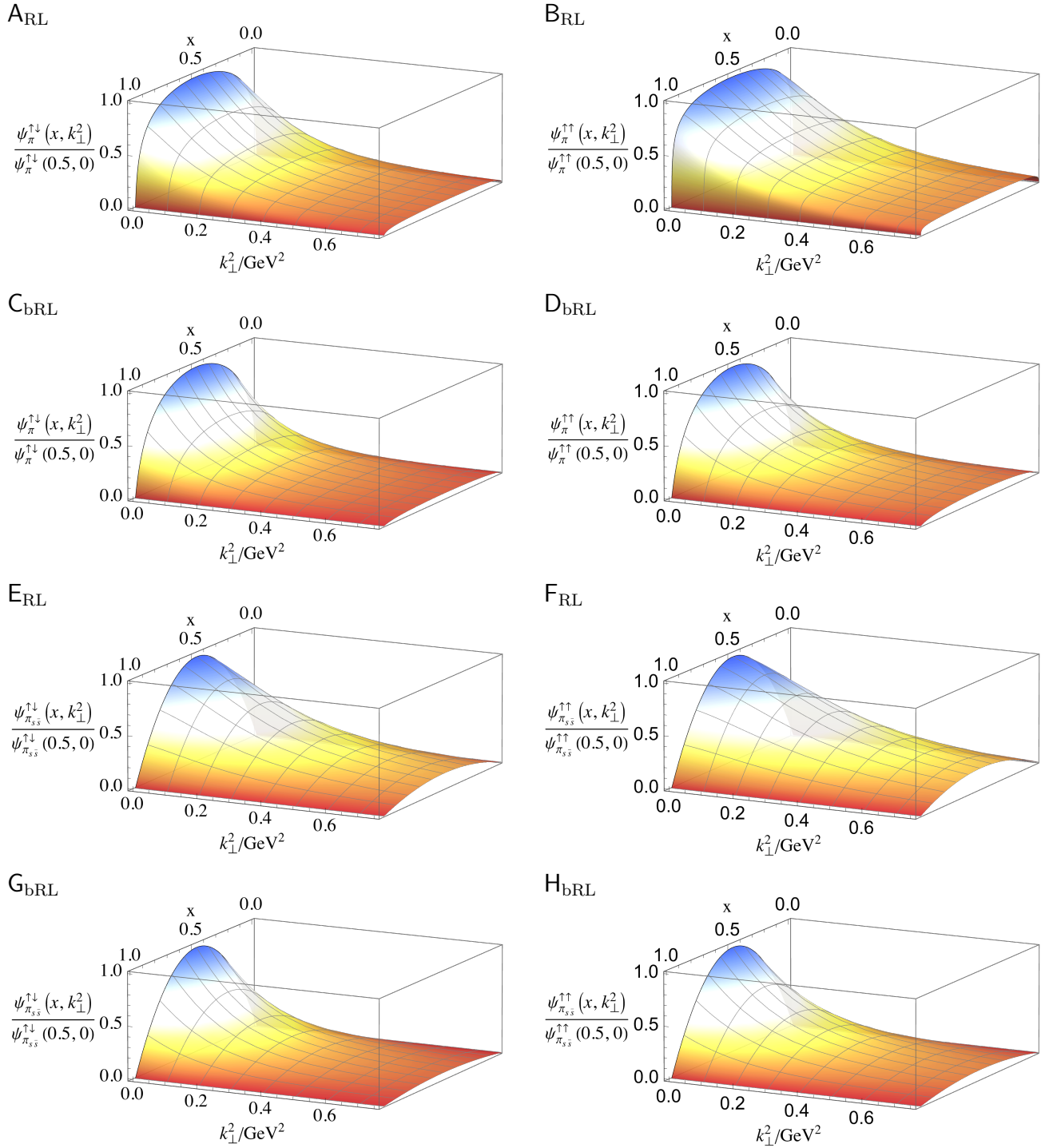


FIG. 3. LFWFs reconstructed from their Mellin moments, expressed by Eq.(17) and central values of the coefficients in Table II. Each curve is normalised by its peak size, determined by the associated values of ρ , $a_0^L + c_0^L$ in Table II. Panel A. π RL, spins antialigned. Panel B. π RL, spins aligned. Panel C. π bRL, spins antialigned. Panel D. π bRL, spins aligned. Panel E. $\pi_{s\bar{s}}$ RL, spins antialigned. Panel F. $\pi_{s\bar{s}}$ RL, spins aligned. Panel G. $\pi_{s\bar{s}}$ bRL, spins antialigned. Panel H. $\pi_{s\bar{s}}$ bRL, spins aligned.

additional dynamical EHM effects captured by the bRL kernel work to enhance the k_\perp^2 support of the $\mathcal{L} = 1$ component of the LFWF.

(b) Turning to the quark current mass dependence, RL

truncation results show large sensitivity to \hat{m} : for both LFWF components, increasing \hat{m} leads to a more dilated k_\perp^2 profile. In contrast, bRL predicts a modest dilation of the $\hat{m}_s \psi_n^0(x, k_\perp^2)$ profile when

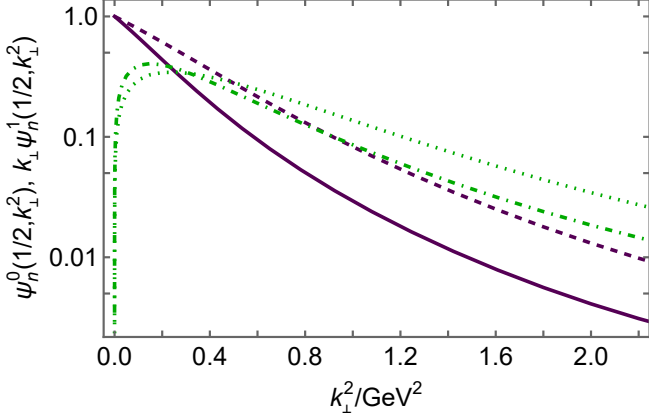
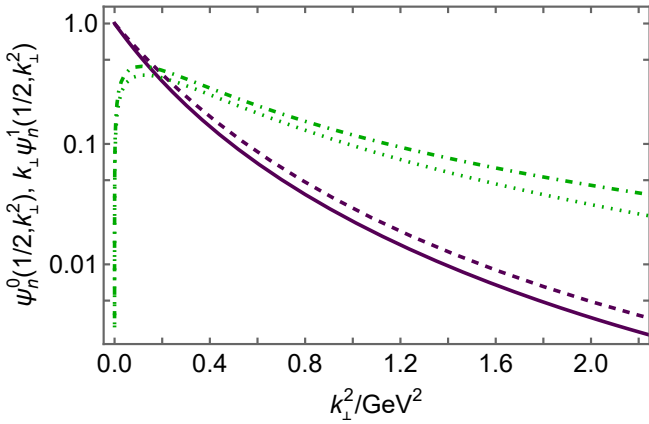
A_{RL}B_{bRL}

FIG. 4. LFWFs for the π and $\pi_{s\bar{s}}$. Panel A – RL truncation; and Panel B – bRL truncation. Legend, both panels: solid purple – ψ_π^0 and dashed purple – $\psi_{\pi_{s\bar{s}}}^0$; and dot-dashed green – $|k_\perp|\psi_\pi^1$ and dotted green – $|k_\perp|\psi_{\pi_{s\bar{s}}}^1$. Further, in each panel, the LFWFs are normalised by the appropriate value of $\psi^0(1/2, 0)$, so the results are dimensionless and the k_\perp^2 -dependence is directly comparable. This is the meaning of the subscript n on the ordinate labels.

compared with that of the kindred \hat{m} amplitude: evidently, with the enhancement of EHM, the relative impact of Higgs-generated mass is smaller.

More strikingly, bRL delivers an inversion of the $|k_\perp|\psi_n^1(x, k_\perp^2)$ profile ordering when compared with the RL results. This further highlights the impact of EHM in the light quark sector: bRL enhances light-quark orbital angular momentum on $k_\perp^2 \gtrsim (0.6 \text{ GeV})^2$.

Given Eq.(9), then one should expect EHM, expressed via the bRL kernel, to have an impact on the k_\perp^2 profile of the TMD, with the importance of the $\mathcal{L} = 1$ contribution being significantly amplified.

V. TMDs

Using the LFWFs in Fig. 3 and Eq. (9), one obtains the TMDs depicted in Fig. 5. Remarks (i) – (iii) and (a), (b) in Sec. IV are also qualitatively applicable to the TMDs.

Analyses in perturbative QCD predict [76] that, on $k_\perp^2 \gg m_N^2$, $\psi_5^0(x, k_\perp^2)$ and $k_\perp^2 \psi_5^1(x, k_\perp^2)$ behave as $1/k_\perp^2$ up to (damping) $\ln k_\perp^2$ corrections. Such behaviour is also expressed in the CSM results described above; hence, the meson TMDs behave as follows:

$$f_1(x, k_\perp^2) \stackrel{k_\perp^2 \gg m_N^2}{\propto} \frac{1}{k_\perp^4 (\ln k_\perp^2)^\gamma}, \quad (20)$$

where $0 < \gamma < 1$ is an anomalous dimension. Whilst $\int dx \int d^2 k_\perp f_1(x, k_\perp^2) = 1 < \infty$ in such circumstances, the mean k_\perp^2 integral is not, *viz.*

$$\langle k_\perp^2 \rangle = \int dx \int d^2 k_\perp k_\perp^2 f_1(x, k_\perp^2) \stackrel{\text{QCD}}{\propto} \infty. \quad (21)$$

Notwithstanding that, if one were to find that an exponential in k_\perp^2 (often called Gaussian) did provide a good approximation to the TMD on $k_\perp^2 \lesssim m_N^2$ – as is common in phenomenology [86], then one could define an effective mean- k_\perp^2 as follows, with $N_0 = \int dx f_1(x, k_\perp^2 = 0)$:

$$\langle k_\perp^2 \rangle_{\text{eff}} = \left[-\frac{1}{N_0} \int dx \frac{d}{dk_\perp^2} f_1(x, k_\perp^2) \right]^{-1} \bigg|_{k_\perp^2=0}, \quad (22)$$

irrespective of the true large- k_\perp^2 behaviour.

Returning to the TMDs in Fig. 5, it is worth identifying the domain on which a k_\perp^2 -exponential dependence may serve as a valid approximation. To that end, we have identified the values of k_\perp^2 at which the relative difference between a low- k_\perp^2 exponential fit is accurate in ratio to within 20% and to within a factor of 2. The domains are bounded above by the values listed in the first two rows of the following array:

| | π^{RL} | π^{bRL} | $\pi_{s\bar{s}}^{\text{RL}}$ | $\pi_{s\bar{s}}^{\text{bRL}}$ |
|--|-------------------|--------------------|------------------------------|-------------------------------|
| $\sqrt{\langle k_\perp^2 \rangle_{20\%}}/\text{GeV}$ | 0.89 | 0.58 | 1.23 | 0.59 |
| $\sqrt{\langle k_\perp^2 \rangle_{100\%}}/\text{GeV}$ | 1.09 | 0.75 | 1.44 | 0.77 |
| $(4/\pi)\langle k_\perp ^2 \rangle^2 / \langle k_\perp^2 \rangle$ | 0.98 | 0.93 | 0.99 | 0.93 |
| $\sqrt{\langle k_\perp^2 \rangle_{\text{eff}}^{\mathcal{L}=0}}/\text{GeV}$ | 0.36 | 0.28 | 0.47 | 0.31 |
| $\sqrt{\langle k_\perp^2 \rangle_{\text{eff}}}/\text{GeV}$ | 0.45 | 0.37 | 0.55 | 0.37 |

so, whilst RL truncation results support a k_\perp^2 -exponential representation over an integration domain that is potentially useful for phenomenology, the bRL predictions indicate a far more limited domain of validity.

In phenomenology, a different measure is commonly used to estimate the reliability of an exponential in k_\perp^2 Ansatz. Namely, were such a profile to be a sound representation, then one would have $\langle |k_\perp|^2 \rangle = (\pi/4)\langle k_\perp^2 \rangle$. This measure is explicated in the third row of Eq.(23). (The results were estimated by integrating on $0 \leq k_\perp^2 \leq$

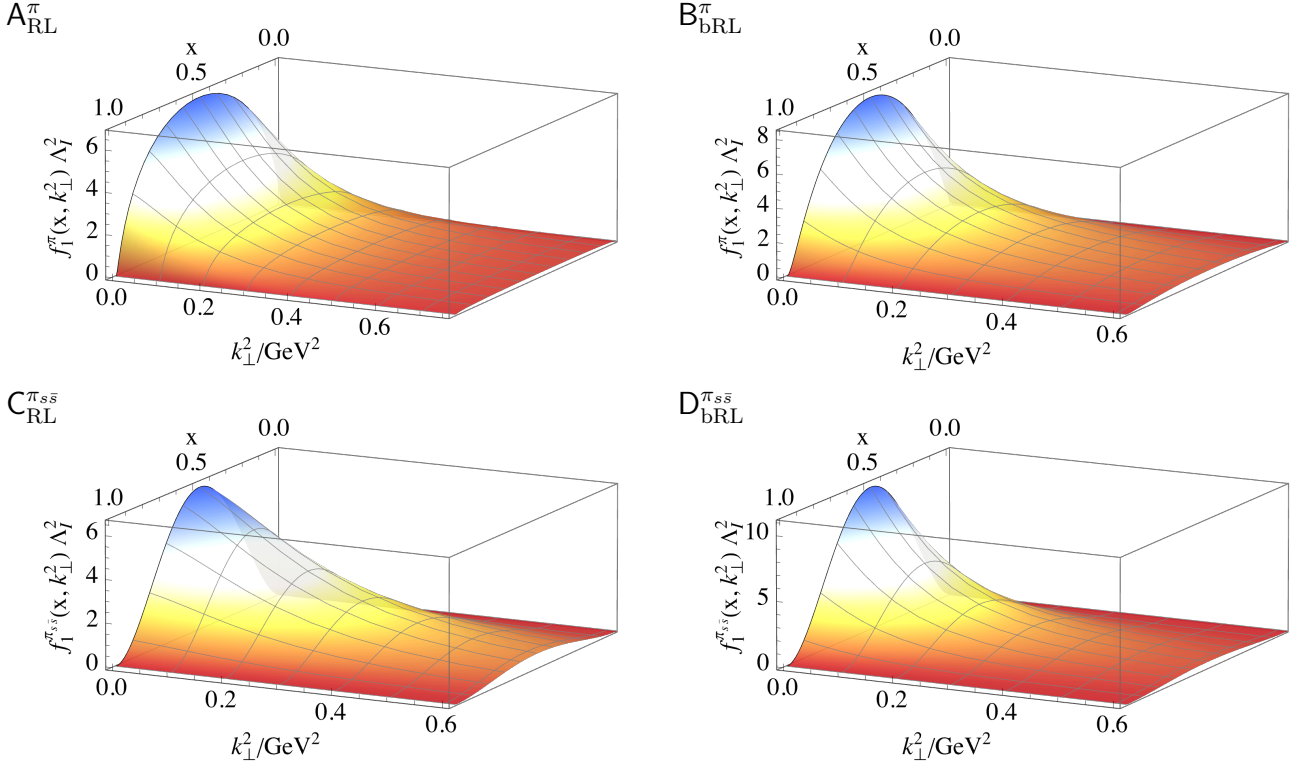


FIG. 5. Helicity-independent TMDs obtained from LFWFs in Fig. 3. In each case, normalisation guarantees Eq. (11). Panel A. π RL. Panel B. π bRL. Panel C. $\pi_{s\bar{s}}$ RL. Panel D. $\pi_{s\bar{s}}$ bRL.

$k_{\perp \text{mf}}^2$.) Evidently, consistent with the first two rows, whilst RL truncation supports such an *Ansatz* over a domain of relevance to phenomenology, bRL does not. Given that bRL is the more realistic truncation, then an exponential in k_{\perp}^2 TMD is not supported by direct calculations.

The bottom two rows of the array in Eq. (23) record values of the effective mean- k_{\perp}^2 , defined in Eq. (22). Row 4 lists the results obtained using only the $\mathcal{L} = 0$ component of the LFWFs and row 5 is the complete result, calculated with both angular momentum pieces. The impact of the $\mathcal{L} = 1$ component is larger for light quarks and largest (32% increase) for the π in bRL truncation.

Regarding RL results, the inflation of the k_{\perp}^2 domain of support seen in Fig. 5C relative to that in Fig. 5A is expressed in a larger mean k_{\perp}^2 . Equally, the similar support ranges of the bRL π and $\pi_{s\bar{s}}$ TMDs translate into practically identical mean- k_{\perp}^2 values.

It is worth looking closer at the k_{\perp}^2 dependence. Considering also momenta $k_{\perp}^2 > 0.6 \text{ GeV}^2$, *viz.* the domain $0 < k_{\perp}^2 \leq k_{\perp \text{mf}}^2$, with $k_{\perp \text{mf}}^2$ being the maximum momentum-squared used in fitting Eq. (17) – see Appendix A, one finds that the ratio $f_1^\pi(x, k_{\perp}^2)/f_1^{\pi_{s\bar{s}}}(x, k_{\perp}^2)$ decreases uniformly with increasing k_{\perp}^2 when RL LFWFs are used. In contrast, with bRL LFWFs on this domain, $f_1^\pi(x, k_{\perp}^2)/f_1^{\pi_{s\bar{s}}}(x, k_{\perp}^2)$ increases uniformly, with increasing k_{\perp}^2 , at first slowly, consistent with the mean- k_{\perp}^2 values

in Eq. (23). Thus, as signalled by the discussion of the LFWFs in Sec. IV, RL and bRL predict different relative behaviour between π and $\pi_{s\bar{s}}$ TMDs on the available domain of precise k_{\perp}^2 results: RL sees EHM strength diluted by Higgs-boson mass effects even at slightly inflated light-quark masses; whereas the bRL kernel predicts that EHM predominates over Higgs-boson effects on a much larger domain of current masses. This is largely because EHM expands the k_{\perp}^2 domain on which the $\mathcal{L} = 1$ component is dominant, increases its magnitude, and inverts the ordering of that magnitude in π *cf.* $\pi_{s\bar{s}}$.

VI. SUMMARY AND PERSPECTIVE

Working from Poincaré-covariant Bethe-Salpeter wave functions for the pion and a fictitious partner state, $\pi_{s\bar{s}}$, in which the valence degrees of freedom both have current masses around 0.1 GeV , we delivered predictions for the light-front wave functions (LFWFs) of these systems. In each case, the Bethe-Salpeter wave function was projected onto the light front and the pointwise behaviour of the LFWF was reconstructed from its six lowest-order k_{\perp}^2 -dependent Mellin moments, $\langle x^m \rangle(k_{\perp}^2)$, $m = 0, 1, \dots, 5$. Both components, valence spin-antialigned ($\mathcal{L} = 0$) and valence spin-aligned ($\mathcal{L} = 1$), were computed and combined to produce the complete LFWF for each bound state.

In completing this analysis, two distinct Bethe-Salpeter kernels were used. Namely, that obtained at leading order in a widely used symmetry-preserving, systematic truncation scheme (rainbow-ladder, RL) and a novel form (bRL), constructed nonperturbatively, which incorporates dynamical effects driven by physics underlying the emergence of hadron mass (EHM). By many measures, the bRL kernel provides the more realistic representation of meson structure.

The following features of the LFWFs are worth highlighting. Considering the ratios $\langle x^m \rangle (k_\perp^2) / \langle x^0 \rangle (k_\perp^2)$, $m = 1, \dots, 5$, for both LFWF spin projections [Fig. 2], then when calculated using the RL kernel, they are all approximately k_\perp^2 -independent, with each taking a value that is a fair match with the associated moment of the system's distribution amplitude (DA). Using instead the bRL kernel, the ratios are constants which are practically indistinguishable from the related DA moments. These outcomes are true for both systems. Hence, their LFWFs can be written in a separable form [Eq. (14), (17)], with this being a reasonable approximation for RL results and a pointwise reliable representation of bRL LFWFs.

Regarding the reconstructed LFWFs themselves [Fig. 3], the $\mathcal{L} = 1$ component is important in all cases. Therefore, its omission delivers a poor approximation. Significant misrepresentations can nevertheless be avoided in integrated quantities, like collinear distribution functions, because both LFWF spin projections are separable, with the dependence on light-front x being the same in both cases. Notably, the realistic bRL kernel produces much stronger $\mathcal{L} = 1$ components in both systems [Fig. 4 and associated discussion].

Naturally, these features of the LFWF are expressed in the associated helicity-independent transverse momentum dependent distribution functions (TMDs) [Sec. V]. Of particular note are the impacts of the bRL kernel. Whereas RL results are compatible with an exponential in k_\perp^2 (Gaussian) *Ansatz* because EHM effects are underestimated, the realistic bRL kernel delivers a more complex LFWF to which a Gaussian provides, at best, only a rough guide to the pointwise k_\perp^2 dependence. The phenomenological reliability of Gaussian *Ansätze* should therefore not be too greatly depended upon.

With a well-grounded pion LFWF in hand, one may now, *e.g.*, revisit existing, exploratory studies of the pion Boer-Mulders (BM) function [87] and work toward a realistic picture of the dependence of pion observables on the transverse spin of its valence constituents. Along the way, one might also learn about the true efficacy of eikonal approximations in estimating the magnitude of the final-state interactions between struck and spectator degrees-of-freedom that are necessary to obtain a nonzero BM function. Such information could be valuable in understanding analogous features of, and influences on, baryon structure.

ACKNOWLEDGMENTS

We thank K. Raya for constructive comments. Work supported by: National Natural Science Foundation of China, grant no. 12135007; Helmholtz-Zentrum Dresden-Rossendorf, under the High Potential Programme; and Ministerio Español de Ciencia, Innovación y Universidades (MICINN) grant no. PID2022-140440NB-C22.

Appendix A: Fitting procedure and uncertainty analysis

For each system considered, one has a set of k_\perp^2 -dependent Mellin moment curves, $\{(j, \langle x^j \rangle (k_\perp^2))\}_{j=0}^{N_x}$. We use $N_x = 5$. In fitting, we introduce a discrete set of $N_k = 40$ k_\perp^2 values, evenly spaced on $0 < k_\perp^2 / \text{GeV}^2 \leq 3 =: k_{\perp \text{mf}}^2$. (We have established that $N_k = 40$ is sufficient to obtain converged results.) We then choose to minimise the following χ^2 function:

$$\chi^2(\vec{\theta}) = \{a_0^\mathcal{L}, b_1^\mathcal{L}, b_2^\mathcal{L}, c_0^\mathcal{L}, d_1^\mathcal{L}, m_2^\mathcal{L}, m_3^\mathcal{L}, m_4^\mathcal{L}, m_5^\mathcal{L}\} \\ = \sum_i^{N_k} \sum_{j=2}^{N_x} \left[\int_0^1 dx x^j \psi_5^\mathcal{L}(x, k^2) - \langle x^j \rangle (k^2) \right]^2 \quad (\text{A1a})$$

$$\stackrel{\text{separable}}{=} \sum_i^{N_k} \sum_{j=2}^{N_x} \left[p_5^\mathcal{L}(k^2) \int_0^1 dx x^j \varphi_5^\mathcal{L}(x) - \langle x^j \rangle^\mathcal{L}(k^2) \right]^2 \quad (\text{A1b})$$

$$= \sum_i^{N_k} \sum_{j=2}^{N_x} \left[p_5^\mathcal{L}(k^2) m_j^\mathcal{L} - \langle x^0 \rangle^\mathcal{L}(k^2) \frac{\langle x^j \rangle^\mathcal{L}(k^2)}{\langle x^0 \rangle^\mathcal{L}(k^2)} \right]^2, \quad (\text{A1c})$$

where we have introduced

$$m_j^\mathcal{L} = \int_0^1 dx x^j \varphi_5^\mathcal{L}(x) \quad (\text{A2})$$

and the sum begins at $j = 2$ because $m_0 = 1$ (DA normalisation) and $m_1 = 1/2$ (DA symmetry under $x \leftrightarrow [1-x]$). For the pion, the moment ratios in Eq. (A1c) are drawn in Fig. 2.

N.B. Although Fig. 2 shows that, for all intents and purposes, the LFWF x -profiles satisfy $\varphi_5^0(x) = \varphi_5^1(x)$, in this Appendix, we elect to provide additional numerical validation of that result by treating the moments in Eq. (A2) as \mathcal{L} -dependent fitting parameters. As we shall find – see Table III below, the returned best-fit values satisfy $m_j^0 = m_j^1$ within mutual uncertainties. With this, one confirms $\varphi_5^0(x) = \varphi_5^1(x)$.

Hereafter, one has a sum of many squares, which must be minimised. In this χ^2 minimisation process, there are nine parameters for $\mathcal{L} = 0$ and seven for $\mathcal{L} = 1$. We denote the results by $\vec{\theta} = \vec{\theta}_f = (a_{0f}^\mathcal{L}, b_{1f}^\mathcal{L}, b_{2f}^\mathcal{L}, c_{0f}^\mathcal{L}, d_{1f}^\mathcal{L}, m_{2f}^\mathcal{L}, m_{3f}^\mathcal{L}, m_{4f}^\mathcal{L}, m_{5f}^\mathcal{L})$ and list their values in Tables II, III. Working with the values in Table III, one obtains the results for $\rho_5^\mathcal{L}$ listed in Table II

TABLE III. Moments obtained via minimisation of Eq. (A1) for the truncations and systems considered herein. The last row lists these moments for the asymptotic DA. Associated correlation matrices are listed in Eqs. (A7)–(A22).

| φ_{5R}^L | m_2^L | m_3^L | m_4^L | m_5^L |
|--|------------|------------|------------|------------|
| $\psi_{\pi, \text{RL}}^{\uparrow\downarrow}$ | 0.3171(42) | 0.2258(41) | 0.1721(41) | 0.1372(41) |
| $\psi_{\pi, \text{RL}}^{\uparrow\uparrow}$ | 0.3217(24) | 0.2325(24) | 0.1809(24) | 0.1481(24) |
| $\psi_{\pi, \text{bRL}}^{\uparrow\downarrow}$ | 0.3096(31) | 0.2144(31) | 0.1594(31) | 0.1244(30) |
| $\psi_{\pi, \text{bRL}}^{\uparrow\uparrow}$ | 0.3077(13) | 0.2116(13) | 0.1561(13) | 0.1208(13) |
| $\psi_{\pi s\bar{s}, \text{RL}}^{\uparrow\downarrow}$ | 0.3008(49) | 0.2011(48) | 0.1441(47) | 0.1084(47) |
| $\psi_{\pi s\bar{s}, \text{RL}}^{\uparrow\uparrow}$ | 0.2997(42) | 0.1995(41) | 0.1421(41) | 0.1061(41) |
| $\psi_{\pi s\bar{s}, \text{bRL}}^{\uparrow\downarrow}$ | 0.2983(32) | 0.1976(31) | 0.1403(31) | 0.1047(31) |
| $\psi_{\pi s\bar{s}, \text{bRL}}^{\uparrow\uparrow}$ | 0.2964(17) | 0.1946(17) | 0.1370(17) | 0.1013(17) |
| φ_{as} | 0.3 | 0.2 | 0.143 | 0.107 |

by simple one-variable minimisation of moment comparisons.

The Hessian matrix associated with the above χ^2 minimisation procedure is

$$[\mathcal{H}_{ij}] = \left[\frac{\partial}{\partial \theta_i} \frac{\partial}{\partial \theta_j} \chi^2(\theta) \right] \Big|_{\theta=\theta_t}. \quad (\text{A3})$$

As usual, with the Hessian in hand, we take the uncertainty in each fitting parameter to be

$$\sigma_i = \sqrt{[\mathcal{H}^{-1}]_{ii}}, \quad \text{no sum on } i, \quad (\text{A4})$$

and the associated correlation matrix is obtained as

$$[C]_{ij} = [H^{-1}]_{ij} / \sqrt{[H^{-1}]_{ii}[H^{-1}]_{jj}}, \quad (\text{A5})$$

again with no sum on repeated indices.

The uncertainties on each reconstruction parameter are listed in Tables II, III. Regarding Table III, within any reasonable understanding of the precision of our results, there is no meaningful difference between $\pi_{s\bar{s}}$ moments and those of φ_{as} . This outcome confirms the analysis in Refs. [82–84].

Calculated results for the correlation matrices follow. In all cases, the result is block diagonal:

$$\begin{array}{c|c} \psi_5^L & \\ \hline C_{5p}^L & 0 \\ 0 & C_{5m}^L \end{array} \quad (\text{A6})$$

One will see that the moments in Eq. (A2) are practically linearly independent.

1. Pion

$$C_{\pi p, \text{RL}}^{\uparrow\downarrow} \begin{array}{c|ccccc} & a_0^0 & b_1^0 & b_2^0 & c_0^0 & d_1^0 \\ \hline a_0^0 & 1 & -0.92 & -0.50 & -0.99 & 0.81 \\ b_1^0 & -0.92 & 1 & 0.72 & 0.92 & -0.60 \\ b_2^0 & -0.50 & -0.72 & 1 & 0.50 & -0.26 \\ c_0^0 & -0.99 & 0.92 & 0.50 & 1 & -0.78 \\ d_1^0 & 0.81 & 0.60 & -0.26 & -0.78 & 1 \end{array} \quad (\text{A7})$$

$$C_{\pi m, \text{RL}}^{\uparrow\downarrow} \begin{array}{c|cccc} & m_2^0 & m_3^0 & m_4^0 & m_5^0 \\ \hline m_2^0 & 1 & 0.05 & 0.04 & 0.03 \\ m_3^0 & 0.05 & 1 & 0.03 & 0.02 \\ m_4^0 & 0.04 & 0.03 & 1 & 0.02 \\ m_5^0 & 0.03 & 0.02 & 0.02 & 1 \end{array} \quad (\text{A8})$$

$$C_{\pi p, \text{RL}}^{\uparrow\uparrow} \begin{array}{c|ccc} & a_1^0 & b_1^1 & b_2^1 \\ \hline a_1^0 & 1 & 0.54 & -0.22 \\ b_1^1 & 0.54 & 1 & -0.76 \\ b_2^1 & -0.22 & -0.76 & 1 \end{array} \quad (\text{A9})$$

$$C_{\pi m, \text{RL}}^{\uparrow\uparrow} \begin{array}{c|cccc} & m_2^1 & m_3^1 & m_4^1 & m_5^1 \\ \hline m_2^1 & 1 & 0.06 & 0.04 & 0.04 \\ m_3^1 & 0.06 & 1 & 0.03 & 0.03 \\ m_4^1 & 0.04 & 0.03 & 1 & 0.02 \\ m_5^1 & 0.04 & 0.03 & 0.02 & 1 \end{array} \quad (\text{A10})$$

$$C_{\pi p, \text{bRL}}^{\uparrow\downarrow} \begin{array}{c|ccccc} & a_0^0 & b_1^0 & b_2^0 & c_0^0 & d_1^0 \\ \hline a_0^0 & 1 & 0.92 & -0.50 & -0.99 & 0.82 \\ b_1^0 & -0.92 & 1 & -0.70 & -0.92 & 0.62 \\ b_2^0 & -0.50 & -0.70 & 1 & 0.50 & -0.27 \\ c_0^0 & -0.99 & 0.92 & 0.50 & 1 & -0.79 \\ d_1^0 & 0.82 & 0.62 & -0.27 & -0.79 & 1 \end{array} \quad (\text{A11})$$

$$C_{\pi m, \text{bRL}}^{\uparrow\downarrow} \begin{array}{c|cccc} & m_2^0 & m_3^0 & m_4^0 & m_5^0 \\ \hline m_2^0 & 1 & 0.05 & 0.04 & 0.03 \\ m_3^0 & 0.05 & 1 & 0.03 & 0.02 \\ m_4^0 & 0.04 & 0.03 & 1 & 0.01 \\ m_5^0 & 0.03 & 0.02 & 0.01 & 1 \end{array} \quad (\text{A12})$$

$$C_{\pi p, \text{bRL}}^{\uparrow\uparrow} \begin{array}{c|ccc} & a_1^0 & b_1^1 & b_2^1 \\ \hline a_1^0 & 1 & 0.54 & -0.21 \\ b_1^1 & 0.54 & 1 & -0.72 \\ b_2^1 & -0.21 & -0.72 & 1 \end{array} \quad (\text{A13})$$

$$\begin{array}{c|cccc}
C_{\pi m b, \text{RL}}^{\uparrow\uparrow} & m_2^1 & m_3^1 & m_4^1 & m_5^1 \\
\hline
m_2^1 & 1 & 0.05 & 0.04 & 0.03 \\
m_3^1 & 0.06 & 1 & 0.03 & 0.02 \\
m_4^1 & 0.04 & 0.03 & 1 & 0.01 \\
m_5^1 & 0.03 & 0.02 & 0.01 & 1
\end{array} \quad (\text{A14})$$

2. Heavy pion

$$\begin{array}{c|ccccc}
C_{\pi s \bar{s} p, \text{RL}}^{\uparrow\downarrow} & a_0^0 & b_1^0 & b_2^0 & c_0^0 & d_1^0 \\
\hline
a_0^0 & 1 & 0.92 & -0.48 & 0.99 & 0.81 \\
b_1^0 & 0.92 & 1 & -0.71 & 0.92 & 0.60 \\
b_2^0 & -0.48 & -0.71 & 1 & -0.48 & -0.25 \\
c_0^0 & -0.99 & 0.92 & -0.48 & 1 & 0.77 \\
d_1^0 & 0.81 & 0.60 & -0.25 & 0.77 & 1
\end{array} \quad (\text{A15})$$

$$\begin{array}{c|ccccc}
C_{\pi s \bar{s} m, \text{RL}}^{\uparrow\downarrow} & m_2^0 & m_3^0 & m_4^0 & m_5^0 \\
\hline
m_2^0 & 1 & 0.05 & 0.03 & 0.02 \\
m_3^0 & 0.05 & 1 & 0.02 & 0.02 \\
m_4^0 & 0.03 & 0.02 & 1 & 0.01 \\
m_5^0 & 0.02 & 0.02 & 0.01 & 1
\end{array} \quad (\text{A16})$$

$$\begin{array}{c|ccc}
C_{\pi s \bar{s} p, \text{RL}}^{\uparrow\uparrow} & a_0^1 & b_1^1 & b_2^1 \\
\hline
a_0^1 & 1 & 0.55 & -0.21 \\
b_1^1 & 0.55 & 1 & -0.75 \\
b_2^1 & -0.21 & -0.75 & 1
\end{array} \quad (\text{A17})$$

$$\begin{array}{c|cccc}
C_{\pi s \bar{s} m, \text{RL}}^{\uparrow\uparrow} & m_2^1 & m_3^1 & m_4^1 & m_5^1 \\
\hline
m_2^1 & 1 & 0.05 & 0.03 & 0.02 \\
m_3^1 & 0.05 & 1 & 0.02 & 0.02 \\
m_4^1 & 0.03 & 0.02 & 1 & 0.01 \\
m_5^1 & 0.02 & 0.02 & 0.01 & 1
\end{array} \quad (\text{A18})$$

$$\begin{array}{c|ccccc}
C_{\pi s \bar{s} p, \text{bRL}}^{\uparrow\downarrow} & a_0^0 & b_1^0 & b_2^0 & c_0^0 & d_1^0 \\
\hline
a_0^0 & 1 & 0.92 & 0.50 & -0.99 & 0.82 \\
b_1^0 & 0.92 & 1 & 0.71 & -0.92 & 0.62 \\
b_2^0 & 0.51 & 0.71 & 1 & -0.51 & 0.27 \\
c_0^0 & -0.99 & -0.92 & -0.51 & 1 & -0.79 \\
d_1^0 & 0.82 & 0.61 & 0.27 & -0.79 & 1
\end{array} \quad (\text{A19})$$

$$\begin{array}{c|ccccc}
C_{\pi s \bar{s} m, \text{bRL}}^{\uparrow\downarrow} & m_2^0 & m_3^0 & m_4^0 & m_5^0 \\
\hline
m_2^0 & 1 & 0.04 & 0.03 & 0.02 \\
m_3^0 & 0.04 & 1 & 0.02 & 0.02 \\
m_4^0 & 0.03 & 0.02 & 1 & 0.01 \\
m_5^0 & 0.02 & 0.02 & 0.01 & 1
\end{array} \quad (\text{A20})$$

$$\begin{array}{c|ccc}
C_{\pi s \bar{s} p, \text{bRL}}^{\uparrow\uparrow} & a_0^1 & b_1^1 & b_2^1 \\
\hline
a_0^1 & 1 & 0.55 & -0.22 \\
b_1^1 & 0.55 & 1 & -0.74 \\
b_2^1 & -0.22 & -0.74 & 1
\end{array} \quad (\text{A21})$$

$$\begin{array}{c|cccc}
C_{\pi s \bar{s} m, \text{bRL}}^{\uparrow\uparrow} & m_2^1 & m_3^1 & m_4^1 & m_5^1 \\
\hline
m_2^1 & 1 & 0.04 & 0.03 & 0.02 \\
m_3^1 & 0.04 & 1 & 0.02 & 0.02 \\
m_4^1 & 0.03 & 0.02 & 1 & 0.01 \\
m_5^1 & 0.02 & 0.02 & 0.01 & 1
\end{array} \quad (\text{A22})$$

- [1] O. Denisov, et al., Letter of Intent (Draft 2.0): A New QCD facility at the M2 beam line of the CERN SPS .
- [2] A. C. Aguilar, et al., Pion and Kaon Structure at the Electron-Ion Collider, Eur. Phys. J. A 55 (2019) 190.
- [3] S. J. Brodsky, et al., Strong QCD from Hadron Structure Experiments, Int. J. Mod. Phys. E 29 (08) (2020) 2030006.
- [4] X. Chen, F.-K. Guo, C. D. Roberts, R. Wang, Selected Science Opportunities for the EicC, Few Body Syst. 61

- (2020) 43.
- [5] D. P. Anderle, et al., Electron-ion collider in China, Front. Phys. (Beijing) 16 (6) (2021) 64701.
- [6] J. Arrington, et al., Revealing the structure of light pseudoscalar mesons at the electron-ion collider, J. Phys. G 48 (2021) 075106.
- [7] C. Quintans, The New AMBER Experiment at the CERN SPS, Few Body Syst. 63 (4) (2022) 72.
- [8] Z. Lu, Z. Yu, T. Lin, Y.-T. Liang, R. Wang, W. Chang,

- W. Xiong, Feasibility Study of Pion and Kaon Structure via the Sullivan Process at EicC – arXiv:2512.01720 [hep-ex] .
- [9] T. Horn, C. D. Roberts, The pion: an enigma within the Standard Model, *J. Phys. G.* 43 (2016) 073001.
 - [10] C. D. Roberts, D. G. Richards, T. Horn, L. Chang, Insights into the emergence of mass from studies of pion and kaon structure, *Prog. Part. Nucl. Phys.* 120 (2021) 103883.
 - [11] E. E. Salpeter, H. A. Bethe, A Relativistic equation for bound state problems, *Phys. Rev.* 84 (1951) 1232–1242.
 - [12] S. J. Brodsky, G. P. Lepage, Perturbative Quantum Chromodynamics, *Prog. Math. Phys.* 4 (1979) 255–422.
 - [13] G. 't Hooft, A Two-Dimensional Model for Mesons, *Nucl. Phys. B* 75 (1974) 461–470.
 - [14] L. Chang, I. C. Cloet, J. J. Cobos-Martinez, C. D. Roberts, S. M. Schmidt, P. C. Tandy, Imaging dynamical chiral symmetry breaking: pion wave function on the light front, *Phys. Rev. Lett.* 110 (2013) 132001.
 - [15] H.-M. Choi, C.-R. Ji, Consistency of the light-front quark model with chiral symmetry in the pseudoscalar meson analysis, *Phys. Rev. D* 91 (2015) 014018.
 - [16] S.-S. Xu, L. Chang, C. D. Roberts, H.-S. Zong, Pion and kaon valence-quark parton quasidistributions, *Phys. Rev. D* 97 (2018) 094014.
 - [17] W. de Paula, E. Ydrefors, J. H. Alvarenga Nogueira, T. Frederico, G. Salmè, Observing the Minkowskian dynamics of the pion on the null-plane, *Phys. Rev. D* 103 (1) (2021) 014002.
 - [18] R. M. Moita, J. P. B. C. de Melo, T. Frederico, W. de Paula, Pion inspired by QCD: Nakanishi and light-front integral representations, *Phys. Rev. D* 106 (1) (2022) 016016.
 - [19] L. Albino, I. M. Higuera-Angulo, K. Raya, A. Bashir, Pseudoscalar mesons: Light front wave functions, GPDs, and PDFs, *Phys. Rev. D* 106 (3) (2022) 034003.
 - [20] Y. Li, P. Maris, J. P. Vary, Chiral sum rule on the light front and the 3D image of the pion, *Phys. Lett. B* 836 (2023) 137598.
 - [21] B. Pasquini, S. Rodini, S. Venturini, Valence quark, sea, and gluon content of the pion from the parton distribution functions and the electromagnetic form factor, *Phys. Rev. D* 107 (11) (2023) 114023.
 - [22] Z. Zhu, Z. Hu, J. Lan, C. Mondal, X. Zhao, J. P. Vary, Transverse structure of the pion beyond leading twist with basis light-front quantization, *Phys. Lett. B* 839 (2023) 137808.
 - [23] X. Wang, L. Chang, M. Ding, K. Raya, C. D. Roberts, Symmetry Constraints on Pion Valence Structure – arXiv:2510.23950 [hep.ph] .
 - [24] C. D. Roberts, Strong QCD and Dyson-Schwinger Equations, *IRMA Lect. Math. and Theor. Phys.* 21 (2015) 356–458.
 - [25] G. Eichmann, H. Sanchis-Alepuz, R. Williams, R. Alkofer, C. S. Fischer, Baryons as relativistic three-quark bound states, *Prog. Part. Nucl. Phys.* 91 (2016) 1–100.
 - [26] S.-X. Qin, C. D. Roberts, Impressions of the Continuum Bound State Problem in QCD, *Chin. Phys. Lett.* 37 (12) (2020) 121201.
 - [27] P. Maris, C. D. Roberts, P. C. Tandy, Pion mass and decay constant, *Phys. Lett. B* 420 (1998) 267–273.
 - [28] P. Maris, C. D. Roberts, π and K meson Bethe-Salpeter amplitudes, *Phys. Rev. C* 56 (1997) 3369–3383.
 - [29] L. Chang, C. D. Roberts, Sketching the Bethe-Salpeter kernel, *Phys. Rev. Lett.* 103 (2009) 081601.
 - [30] C. S. Fischer, R. Williams, Probing the gluon self-interaction in light mesons, *Phys. Rev. Lett.* 103 (2009) 122001.
 - [31] S.-X. Qin, C. D. Roberts, S. M. Schmidt, Ward-Green-Takahashi identities and the axial-vector vertex, *Phys. Lett. B* 733 (2014) 202–208.
 - [32] H. J. Munczek, Dynamical chiral symmetry breaking, Goldstone's theorem and the consistency of the Schwinger-Dyson and Bethe-Salpeter Equations, *Phys. Rev. D* 52 (1995) 4736–4740.
 - [33] A. Bender, C. D. Roberts, L. von Smekal, Goldstone Theorem and Diquark Confinement Beyond Rainbow- Ladder Approximation, *Phys. Lett. B* 380 (1996) 7–12.
 - [34] S.-X. Qin, C. D. Roberts, Resolving the Bethe-Salpeter kernel, *Chin. Phys. Lett.* *Express* 38 (7) (2021) 071201.
 - [35] Z.-N. Xu, Z.-Q. Yao, S.-X. Qin, Z.-F. Cui, C. D. Roberts, Bethe-Salpeter kernel and properties of strange-quark mesons, *Eur. Phys. J. A* 59 (3) (2023) 39.
 - [36] Z. N. Xu, Z. Q. Yao, D. Binosi, M. Ding, C. D. Roberts, J. Rodríguez-Quintero, Distribution functions of a radially excited pion, *Eur. Phys. J. C* 85 (3) (2025) 330.
 - [37] C. D. Roberts, S. M. Schmidt, Reflections upon the Emergence of Hadronic Mass, *Eur. Phys. J. ST* 229 (22-23) (2020) 3319–3340.
 - [38] D. Binosi, Emergent Hadron Mass in Strong Dynamics, *Few Body Syst.* 63 (2) (2022) 42.
 - [39] M. Ding, C. D. Roberts, S. M. Schmidt, Emergence of Hadron Mass and Structure, *Particles* 6 (1) (2023) 57–120.
 - [40] M. N. Ferreira, J. Papavassiliou, Gauge Sector Dynamics in QCD, *Particles* 6 (1) (2023) 312–363.
 - [41] K. Raya, A. Bashir, D. Binosi, C. D. Roberts, J. Rodríguez-Quintero, Pseudoscalar Mesons and Emergent Mass, *Few Body Syst.* 65 (2) (2024) 60.
 - [42] P. Achenbach, D. S. Carman, R. W. Gothe, K. Joo, V. I. Mokeev, C. D. Roberts, Electroexcitation of Nucleon Resonances and the Emergence of Hadron Mass, *Symmetry* 17 (7) (2025) 1106.
 - [43] P.-L. Yin, Y.-Z. Xu, Z.-F. Cui, C. D. Roberts, J. Rodríguez-Quintero, All-Orders Evolution of Parton Distributions: Principle, Practice, and Predictions, *Chin. Phys. Lett.* *Express* 40 (9) (2023) 091201.
 - [44] S.-X. Qin, L. Chang, Y.-X. Liu, C. D. Roberts, D. J. Wilson, Interaction model for the gap equation, *Phys. Rev. C* 84 (2011) 042202(R).
 - [45] D. Binosi, L. Chang, J. Papavassiliou, C. D. Roberts, Bridging a gap between continuum-QCD and *ab initio* predictions of hadron observables, *Phys. Lett. B* 742 (2015) 183–188.
 - [46] D. Binosi, L. Chang, J. Papavassiliou, S.-X. Qin, C. D. Roberts, Natural constraints on the gluon-quark vertex, *Phys. Rev. D* 95 (2017) 031501(R).
 - [47] Z. Q. Yao, Y. Z. Xu, D. Binosi, Z. F. Cui, M. Ding, K. Raya, C. D. Roberts, J. Rodríguez-Quintero, S. M. Schmidt, Nucleon gravitational form factors, *Eur. Phys. J. A* 61 (5) (2025) 92.
 - [48] L. Chang, Y.-X. Liu, C. D. Roberts, Y.-M. Shi, W.-M. Sun, H.-S. Zong, Chiral susceptibility and the scalar Ward identity, *Phys. Rev. C* 79 (2009) 035209.
 - [49] S. Navas, et al., Review of particle physics, *Phys. Rev. D* 110 (3) (2024) 030001.
 - [50] J. Singh, Anomalous magnetic moment of light quarks

- and dynamical symmetry breaking, *Phys. Rev. D* 31 (1985) 1097–1108.
- [51] P. J. A. Bicudo, J. E. F. T. Ribeiro, R. Fernandes, The anomalous magnetic moment of quarks, *Phys. Rev. C* 59 (1999) 1107–1112.
 - [52] L. Chang, Y.-X. Liu, C. D. Roberts, Dressed-quark anomalous magnetic moments, *Phys. Rev. Lett.* 106 (2011) 072001.
 - [53] S.-X. Qin, L. Chang, Y.-X. Liu, C. D. Roberts, S. M. Schmidt, Practical corollaries of transverse Ward-Green-Takahashi identities, *Phys. Lett. B* 722 (2013) 384–388.
 - [54] P. Maris, P. C. Tandy, QCD modeling of hadron physics, *Nucl. Phys. Proc. Suppl.* 161 (2006) 136–152.
 - [55] A. Krassnigg, Excited mesons in a Bethe-Salpeter approach, *PoS CONFINEMENT8* (2008) 075.
 - [56] M. S. Bhagwat, A. Krassnigg, P. Maris, C. D. Roberts, Mind the gap, *Eur. Phys. J. A* 31 (2007) 630–637.
 - [57] A. Krassnigg, Survey of $J=0,1$ mesons in a Bethe-Salpeter approach, *Phys. Rev. D* 80 (2009) 114010.
 - [58] N. Nakanishi, A General survey of the theory of the Bethe-Salpeter equation, *Prog. Theor. Phys. Suppl.* 43 (1969) 1–81.
 - [59] G. Grunberg, Renormalization Group Improved Perturbative QCD, *Phys. Lett. B* 95 (1980) 70, [Erratum: *Phys. Lett. B* 110, 501 (1982)].
 - [60] G. Grunberg, Renormalization Scheme Independent QCD and QED: The Method of Effective Charges, *Phys. Rev. D* 29 (1984) 2315.
 - [61] A. Deur, S. J. Brodsky, C. D. Roberts, QCD Running Couplings and Effective Charges, *Prog. Part. Nucl. Phys.* 134 (2024) 104081.
 - [62] A. Deur, V. Burkert, J. P. Chen, W. Korsch, Experimental determination of the QCD effective charge $\alpha_{g1}(Q)$, *Particles* 5 (2) (2022) 171–179.
 - [63] M. Gell-Mann, F. E. Low, Quantum electrodynamics at small distances, *Phys. Rev.* 95 (1954) 1300–1312.
 - [64] Y. L. Dokshitzer, Calculation of the Structure Functions for Deep Inelastic Scattering and e^+e^- Annihilation by Perturbation Theory in Quantum Chromodynamics. (In Russian), *Sov. Phys. JETP* 46 (1977) 641–653.
 - [65] V. N. Gribov, L. N. Lipatov, Deep inelastic electron scattering in perturbation theory, *Phys. Lett. B* 37 (1971) 78–80.
 - [66] L. N. Lipatov, The parton model and perturbation theory, *Sov. J. Nucl. Phys.* 20 (1975) 94–102.
 - [67] G. Altarelli, G. Parisi, Asymptotic Freedom in Parton Language, *Nucl. Phys. B* 126 (1977) 298–318.
 - [68] Z. F. Cui, M. Ding, J. M. Morgado, K. Raya, D. Binosi, L. Chang, F. De Soto, C. D. Roberts, J. Rodríguez-Quintero, S. M. Schmidt, Emergence of pion parton distributions, *Phys. Rev. D* 105 (9) (2022) L091502.
 - [69] Y.-Z. Xu, K. Raya, Z.-F. Cui, C. D. Roberts, J. Rodríguez-Quintero, Empirical Determination of the Pion Mass Distribution, *Chin. Phys. Lett. Express* 40 (4) (2023) 041201.
 - [70] Y. Lu, Y.-Z. Xu, K. Raya, C. D. Roberts, J. Rodríguez-Quintero, Pion distribution functions from low-order Mellin moments, *Phys. Lett. B* 850 (2024) 138534.
 - [71] Z.-N. Xu, D. Binosi, C. Chen, K. Raya, C. D. Roberts, J. Rodríguez-Quintero, Kaon distribution functions from empirical information, *Phys. Lett. B* 865 (2025) 139451.
 - [72] I. C. Cloet, L. Chang, C. D. Roberts, S. M. Schmidt, P. C. Tandy, Pion distribution amplitude from lattice-QCD, *Phys. Rev. Lett.* 111 (2013) 092001.
 - [73] Z.-F. Cui, M. Ding, F. Gao, K. Raya, D. Binosi, L. Chang, C. D. Roberts, J. Rodríguez-Quintero, S. M. Schmidt, Kaon and pion parton distributions, *Eur. Phys. J. C* 80 (2020) 1064.
 - [74] G. S. Bali, V. M. Braun, S. Bürger, M. Göckeler, M. Gruber, F. Hutzler, P. Korcyl, A. Schäfer, A. Sternbeck, P. Wein, Light-cone distribution amplitudes of pseudoscalar mesons from lattice QCD, *JHEP* 08 (2019) 065, [Addendum: *JHEP* 11, 037 (2020)].
 - [75] K. Raya, Z.-F. Cui, L. Chang, J.-M. Morgado, C. D. Roberts, J. Rodríguez-Quintero, Revealing pion and kaon structure via generalised parton distributions, *Chin. Phys. C* 46 (26) (2022) 013105.
 - [76] G. P. Lepage, S. J. Brodsky, Exclusive Processes in Perturbative Quantum Chromodynamics, *Phys. Rev. D* 22 (1980) 2157–2198.
 - [77] G. P. Lepage, S. J. Brodsky, Exclusive Processes in Quantum Chromodynamics: Evolution Equations for Hadronic Wave Functions and the Form-Factors of Mesons, *Phys. Lett. B* 87 (1979) 359–365.
 - [78] A. V. Efremov, A. V. Radyushkin, Factorization and Asymptotical Behavior of Pion Form-Factor in QCD, *Phys. Lett. B* 94 (1980) 245–250.
 - [79] Z. F. Cui, M. Ding, J. M. Morgado, K. Raya, D. Binosi, L. Chang, J. Papavassiliou, C. D. Roberts, J. Rodríguez-Quintero, S. M. Schmidt, Concerning pion parton distributions, *Eur. Phys. J. A* 58 (1) (2022) 10.
 - [80] H. Y. Xing, M. Ding, Z. F. Cui, A. V. Pimikov, C. D. Roberts, S. M. Schmidt, Constraining the pion distribution amplitude using Drell-Yan reactions on a proton, *Phys. Lett. B* 849 (2024) 138462.
 - [81] C. D. Roberts, Hadron Structure Using Continuum Schwinger Function Methods, *Few Body Syst.* 64 (3) (2023) 51.
 - [82] M. Ding, F. Gao, L. Chang, Y.-X. Liu, C. D. Roberts, Leading-twist parton distribution amplitudes of S-wave heavy-quarkonia, *Phys. Lett. B* 753 (2016) 330–335.
 - [83] M. Chen, M. Ding, L. Chang, C. D. Roberts, Mass-dependence of pseudoscalar meson elastic form factors, *Phys. Rev. D* 98 (2018) 091505(R).
 - [84] M. Ding, K. Raya, A. Bashir, D. Binosi, L. Chang, M. Chen, C. D. Roberts, $\gamma^*\gamma \rightarrow \eta, \eta'$ transition form factors, *Phys. Rev. D* 99 (2019) 014014.
 - [85] R. Zhang, C. Honkala, H.-W. Lin, J.-W. Chen, Pion and kaon distribution amplitudes in the continuum limit, *Phys. Rev. D* 102 (9) (2020) 094519.
 - [86] R. Boussarie, et al., *TMD Handbook* – arXiv:2304.03302 [hep-ph] .
 - [87] D. Boer, P. Mulders, Time reversal odd distribution functions in leptonproduction, *Phys. Rev. D* 57 (1998) 5780–5786.